

Deep Image-Based Adaptive BRDF Measure

Wen Cao¹

Media and Information Technology, Department of Science and Technology, Linköping University,
SE-601 74 Norrköping, Sweden

Keywords: BRDF Measure, Adaptive, Deep Learning.

Abstract: Efficient and accurate measurement of the bi-directional reflectance distribution function (BRDF) plays a key role in realistic image rendering. However, obtaining the reflectance properties of a material is both time-consuming and challenging. This paper presents a novel iterative method for minimizing the number of samples required for high quality BRDF capture using a gonio-reflectometer setup. The method is a two-step approach, where the first step takes an image of the physical material as input and uses a lightweight neural network to estimate the parameters of an analytic BRDF model. The second step adaptive sample the measurements using the estimated BRDF model and an image loss to maximize the BRDF representation accuracy. This approach significantly accelerates the measurement process while maintaining a high level of accuracy and fidelity in the BRDF representation.

1 INTRODUCTION


The bidirectional reflectance distribution function (BRDF) (Nicodemus, 1965), is a fundamental concept in computer graphics, representing the interaction of light with a material. It is a four-dimensional function that defines the relationship between incoming and outgoing light directions at a material surface. BRDFs can be represented either by analytic models (Cook and Torrance, 1982; Phong, 1975) or by tabulated measurements for every pair of incident and outgoing angles (Matusik et al., 2003), with each approach having its own advantages and disadvantages. The capture of real, physical BRDFs is an important tool in many applications ranging from photo-realistic image synthesis and predictive appearance visualization—such as in additive manufacturing—to enabling accurate sensor simulation and modeling of scattering behaviors in industrial processes. However, detailed BRDF measurement is a time-consuming process because it typically requires dense mechanical scanning of light sources and sensors across the entire hemisphere. Several studies (Liu et al., 2023; Dupuy and Jakob, 2018) have been conducted to reduce capture time by taking fewer measurements. Recently, neural approaches (Zhang et al., 2021; Gao et al., 2019) have been proposed to represent synthetic BRDFs from images, primarily by estimating the an-

alytic BRDF parameters.

The objective of this paper is to accelerate BRDF measurements using gonio-reflectometer setups, see e.g. (Nielsen et al., 2015; Foo et al., 1997). To incorporate prior knowledge of the measured material, our method uses a small neural network that takes an image of the material as input to estimate the configuration of a small set of sampling directions to enable efficient BRDF measurement. Specifically, we employ an encoder network to estimate the reflectance parameters of analytic BRDF models from the input image, which are used to adapt the BRDF measurement directions. The method leverages both analytic BRDF models and image-based neural decomposition as priors. These two priors are essential for efficiently utilizing small networks to estimate the adaptive sample distribution.

In summary, we present a novel solution for BRDF measurement with the following key contributions:

- **Lightweight.** Our approach utilizes images to learn priors, eliminating the need for complex measurement procedures. This significantly streamlines the measurement process and establishes an end-to-end pipeline.
- **Adaptive and Accuracy.** Experimental results demonstrate that our image-based adaptive method effectively measure a wide range of materials. Its adaptability leads to highly accurate

¹ <https://orcid.org/0000-0002-2507-7288>

rendered results for each material, outperforming previous methods at some aspects.

2 RELATED WORK

In this section, we review previous work related to BRDF measurement and neural spatially varying bidirectional reflectance distribution function-SVBRDF capture.

BRDF Measurement: is commonly done using gonioreflectometers, which capture the reflectance of realistic materials by controlling mechanical light sources and camera motions (Foo et al., 1997). For example, acquiring the MERL dataset requires totaling approximately 1.46 million samples (Rusinkiewicz, 1998; Matusik et al., 2003). To accelerate the acquisition, several methods and devices have been developed. Nielsen et al. (Nielsen et al., 2015) and Miandji et al. (Miandji et al., 2024) used the measured BRDF Dataset to train a basis to linearly reconstruct the full BRDF samples to accelerate the measurements. Dupuy et al. (Dupuy and Jakob, 2018) used a laser machine to measure the NDF values of materials to adaptive sample the hemisphere domain. Liu et al. (Liu et al., 2023) used a meta-learning method to optimize the sampling count of different BRDF models.

Neural (SV)BRDF Capture. Researchers are exploring deep learning methods to develop lightweight approaches for measuring (SV)BRDF values (Kavoosighafi et al., 2024; Gao et al., 2019). Deschaintre (Deschaintre et al., 2019) used an encoder-decoder network to estimate the normal, diffuse albedo, and roughness images from phone-captured images. Zhang (Zhang et al., 2021) used images as input to predict BRDF values for each pixel based on NeRF output. Zeng (Zeng et al., 2024) used a diffusion framework to decompose RGB images into normal, albedo, roughness, metallicity and diffuse maps.

3 APPROACH

Our method employs a Convolutional Neural Network (CNN) encoder to estimate the BRDF parameters of an analytic model from a single image. Based on the estimated BRDF model, we utilize importance sampling to derive an adaptive sampling pattern for the input material. These sampling values are used to render the estimated image by bilinear interpolation. The rendered images with measured samples are fed back to the sample selector, which calculates the im-

age loss and determines the optimal number of samples for the next iteration as illustrated in Figure 1.

3.1 BRDF Estimation

Drawing inspiration from deep learning techniques used in SVBRDF capture (Deschaintre et al., 2019) from images, we train a convolutional neural network to encode isotropic material images into their corresponding appearance parameters for a set of analytical models. The architecture of the BRDF estimation network is illustrated in Figure 2 and employs sigmoid activation functions for the parameter outputs.

3.1.1 Analytic BRDF

We use the Ward BRDF model (Walter, 2005) parameterized by its diffuse reflection coefficient ρ_d , roughness α and specular reflection coefficient ρ_s to train the network. The isotropic Ward BRDF $f_r(\mathbf{i}, \mathbf{o})$ with incoming direction \mathbf{i} and outgoing direction \mathbf{o} is:

$$f_r(\mathbf{i}, \mathbf{o}) = \frac{\rho_d}{\pi} + \frac{\rho_s}{4\pi\alpha^2\sqrt{\cos\theta_i\cos\theta_o}} e^{-\frac{\tan^2\theta_h}{\alpha^2}} \quad (1)$$

where $\theta_i, \theta_o, \theta_h$ is the incoming angle, outgoing angle, half angle.

To train the encoder network, we use the Loss function of Ward BRDF model as below

$$\mathcal{L}_{\text{loss}} = \|\hat{I} - I\|_1 + \|(\hat{\rho}_d, \hat{\alpha}) - (\rho_d, \alpha)\|_1 \quad (2)$$

where I represents the rendered image based on the BRDF parameters. L1 loss is used for both images and parameters.

3.1.2 Measured BRDF

We use the Measured BRDFs Dataset (MERL) (Matusik et al., 2003) for training and validation. We predict roughness, α , for each image by training from the neural BRDF network from scratch.

$$f_r(\mathbf{i}, \mathbf{o}) = f_{ggx}^l(\alpha) \quad (3)$$

where f_{ggx}^l is the microfacet BRDF model (Zhang et al., 2021) representing the reflectance. We optimize the network to minimize the loss between estimation and ground truth of alpha value and images.

$$\mathcal{L}_{\text{loss}} = \|\hat{I} - I\|_1 + \|(\hat{\alpha}) - (\alpha)\|_2 \quad (4)$$

The ground truth alpha values for each MERL material are derived by fitting their respective total BRDF data to the microfacet BRDF model. Based on the BRDF parameters estimated by the network,

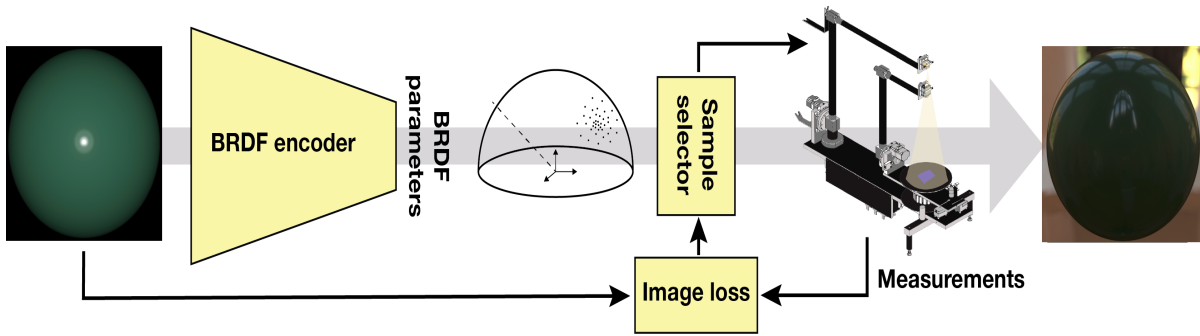


Figure 1: Method Flowchart of Deep Image-based Adaptive Reflectance Measure. For a fixed material, we use its image as input to an encoder network, which then estimates the BRDF parameters for it. An adaptive sampler use these parameters to determine the outgoing direction locations. Finally, we progressively increase the number of these locations to achieve the minimum number of samples required while maintaining high fidelity.

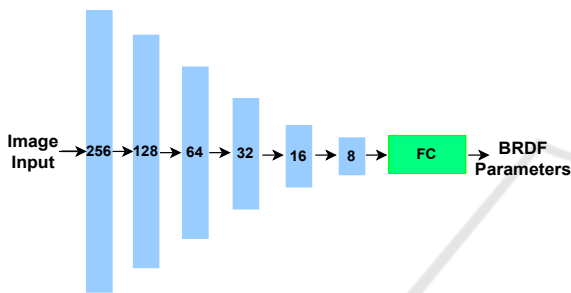


Figure 2: Illustration of the encoder network architecture used for estimating BRDF parameters. Blue boxes denote convolutional layers with batch normalization and ReLU activation functions. The dimensions of these layers are the numbers inside them. The green box represents a fully connected layer outputting the BRDF parameters.

the estimated images \hat{I} are rendered using the Microfacet BRDF model. We employed an L1 loss between the predicted images \hat{I} and the ground truth images I , while an L2 loss was applied to the parameter estimations.

3.2 Adaptive Reflectance Sampling

Using the BRDF estimation network, we are able to derive the BRDF parameters from an input image. We draw inspiration from previous work and utilize the inverted BRDF importance sampling to drive an adaptive sampling distribution of the outgoing hemisphere which is similar to the work of Dupuy et al. (Dupuy and Jakob, 2018; Bai et al., 2023). This adaptive sampling strategy effectively minimizes measurement time by targeting only those directions specified by the input BRDF material pattern. For instance, in the case of a mirror-like material, sampling is concentrated on the delta regions directly opposite the incoming light direction. In contrast, for diffuse materials, a uniform sampling pattern is implemented throughout the hemisphere. In practice, the BRDF

sampling pattern for most materials typically falls between these two extremes. For details on importance sampling, we refer to Bai et al. (Bai et al., 2023).

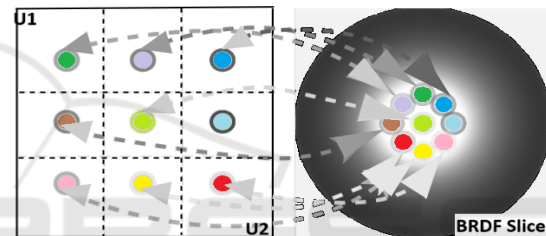


Figure 3: A visualization of the process g in Eq. 5 to calculate the adaptive sampler's position. We start by getting sample points (u_1, u_2) on a uniform grid in the unit square $[0, 1]^2$. The importance sampling process takes a sample point (u_1, u_2) , and maps it to position on a 2D BRDF slice, and reverse wise works by its inverse function.

The rendering equation of general BRDF model is as follows:

$$I(\mathbf{i}) = \int_{\Omega^2} f_r(\mathbf{i}, g(\mathbf{u})) L_i(g(\mathbf{u})) \|J_g(\mathbf{u})\| d\mathbf{u} \quad (5)$$

where L_i is the incident radiance, I_i denotes the radiance reflected in all directions at pixel point \mathbf{i} , J_g is the Jacobian of g .

$$p(\omega_o) = w_d \cdot p_d(\omega_o) + w_s \cdot p_s(\omega_o) \quad (6)$$

where $w_d + w_s = 1$, $p(\omega_o)$ is the PDF of outgoing direction ω_o . The diffuse PDF p_d is a simple cosine-weighted distribution and PDF p_s is the specular distribution based on BRDF specular lobe. The equation g defines the adaptive sampling strategy in the outgoing hemisphere domain according to the specular distribution p_d without the diffuse distribution as Figure 3 and its inverse g^{-1} map the location of BRDF slice back to the unit square which is used in bilinear interpolation to fully evaluate the BRDF values in the rendering function to produce the image.

Thus, we focus on samplers suitable for representing f_r : an invertible function g from random variates $\mathbf{u} \in [0, 1]^2$ into outgoing directions ω_o and its associated probability density function (PDF) $p(\omega_o, \omega_i)$. The shape of p should closely matches f_r to achieve low variance.

3.2.1 Importance Sampling

The importance sampling equation for the Ward BRDF model used in this work is:

$$\begin{aligned} \theta_h &= \arctan(\alpha\sqrt{-\log u_1}) \\ \phi_h &= 2\pi u_2 \end{aligned} \tag{7}$$

where ϕ_h, θ_h is the half angle; u_1, u_2 is the uniform variates on $[0, 1]^2$ (Walter, 2005). We compute the inverse of Equation 7 to evaluate the measured BRDF parameters in the rendering equation using:

$$\begin{aligned} u_1 &= e^{-\frac{\tan^2 \theta_h}{\alpha^2}} \\ u_2 &= \frac{\phi_h}{2\pi} \end{aligned} \tag{8}$$

Then, we use $\omega_o = 2(\omega_h \cdot \omega_i)\omega_h - \omega_i$ to determines the outgoing direction $\omega_o(\phi_h, \theta_h)$.

For the MERL dataset, there is no analytical function for obtaining the PDF. Therefore, we approximate the PDF using the microfacet BRDF model (Dupuy, 2015) and employ its importance sampling method to achieve adaptive measurements. Additionally, we utilize the inverse of this function in the rendering process. Detailed functions and methodologies can be found in Dupuy’s Ph.D. thesis (Dupuy, 2015)

Based on the importance sampling procedures explained above, we adaptively sample the outgoing direction according to the PDF and subsequently use the direction to make a new measurement of the material BRDF. Thus, previous measurements guide the goniometer and facilitate precise and efficient measurement of the input material with reduced capture time. The incoming directions are uniformly sampled within the cosine-weighted hemisphere.

4 IMPLEMENTATION

We use Mitsuba 3.0 (Jakob et al., 2022) and its Python bindings to render images of size 256×256 and PyTorch to implement the neural network.

4.1 Dataset

To train the neural network of the Ward BRDF model, we create a dataset covering the full range of Ward

BRDF parameter- α . Images with varying roughness and diffuse values were rendered using the Ward BRDF function, a single point light source, and a sphere in Mitsuba. The dataset consists of 4,000 training images and 100 test images.

Similarly, for the MERL dataset, we fit each material to the Microfacet BRDF model. We first create datasets by rendering images with varying alpha and albedo values using the Microfacet BRDF model. These images are used to pretrain the BRDF estimation network, addressing the limited amount of measured data in the MERL dataset. We then fine-tune the BRDF estimation network using the MERL training images, with the fitted alpha values serving as ground truth. The Microfacet dataset comprises 40,000 training images and 100 test images, while the MERL dataset includes 85 training images and 15 test images rendered with different materials.

4.2 Estimation

The BRDF estimation network are depicted in Figure 2 . We train the network in Nivida Geforce RTX 4080 with 15GB memory.

We demonstrate that our BRDF estimation network accurately predicts BRDF parameters for both the Ward model and the MERL dataset, as illustrated in Figure 4. For the Ward BRDF model, the network achieves nearly perfect predictions with errors between -0.0015 and 0.0020. For the 15 materials in the MERL test set, the estimation errors range between -0.1 and 0.1. In most BRDF models, albedo represents the base color, while alpha describes the shape of the BRDF reflection lobe. Since the base color is visually evident in our results, we primarily present the network’s alpha estimations in Figure 4.

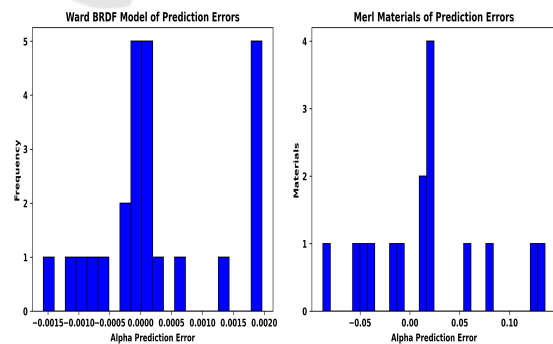


Figure 4: Error distributions for BRDF parameters estimation. It can be seen that the error varies in a small range.

4.3 Sample Count

We treat the number of outgoing directions as hyper-parameters of the entire pipeline. For each material, we optimize the number of samples by the image loss between the rendered images by the measurements and the ground truth.

However we observe that the performance plots based on sample number vary across different materials, as shown in Figure 5. Generally, materials with higher specular reflections require more samples. To minimize the size of the measurements, we set the maximum direction count to 32×32 , as increasing the number of samples beyond this point yields visually negligible improvements for most materials.

For the number of incident directions, we use one ϕ point and eight θ points sampled from a uniform cosine distribution, adhering to the rotational symmetry of isotropic materials. The number of directions was determined based on the work by Dupuy and Jakob (Dupuy and Jakob, 2018).

5 RESULTS

In this section, we present the qualitative results and comparisons with state-of-the-art methods for BRDF acquisition. For quantitative evaluations, we employ metrics as Peak Signal-to-Noise Ratio (PSNR), Root Mean Square Error (RMSE), and mean \mathcal{FLIP} error (Andersson et al., 2020). Additionally, we use \mathcal{FLIP} error maps to visualize the errors in the rendered images.

5.1 Comparison

Here, we compare our method with the state of the art method meta-learning brdf sampling method (Liu et al., 2023). Since Liu’s method learns sample patterns for all materials, its performance does not improve with increased sample counts once highlights are achieved. Additionally, it requires the implementation of a fixed sample count. In contrast, we derive adaptive sampling pattern for each specific input material, allowing the performance to progressively increase as more samples are added.

We show the comparison between our method and Liu’s method in Table 1, using the nine test materials from our test datasets derived from the MERL dataset. For quantitative comparison, we select results from Liu’s method and our results with same sample numbers.

Specifically, Liu’s method uses from 32 to 512 samples within the Rusinkiewicz parameteriza-

tion (Rusinkiewicz, 1998), while our approach adopts a configuration of 1×8 incoming directions(θ_{in}, ϕ_{in}) and from 2×2 to 8×8 outgoing directions(θ_{out}, ϕ_{out}) in spherical coordinates.

Our method consistently produces high-fidelity rendered images across all tests, particularly with an relative high number of samples. In contrast, Liu’s method performs well with fewer samples, but its accuracy declines as the sample count grows. For diffuse and specular materials, our approach performs comparable with Liu’s, as demonstrated by the results in Table 1.

5.2 Evaluation on Different Materials

We show more visual results in Figure 5 with five different materials. We observe that diffuse materials achieve high-quality results with fewer samples, whereas highly specular materials require a larger number of samples to produce good outcomes. The first row and second row are the rendered images using our adaptive measurement method under point lighting and environment lighting, respectively. The fourth rows of Figure 5 shows the \mathcal{FLIP} Error image comparing the second row (rendered images from our method) with the third row (ground truth), where specular materials generally exhibit higher errors. The last row presents the plot of the performance metrics based on sample numbers, illustrating how the sample count is selected for each material as described in subsection 4.3.

6 DISCUSSION

Moreover, additional variants in sample methods and BSDF models could be further explored within this approach.

Sample Method. Normalizing Flows (Müller et al., 2019) is a possible alternative to our adaptive sampler, as it supports both inverse and forward sampling and can be co-optimized with the entire pipeline. Investigating the integration of Normalizing Flows into our sampling strategy could be a valuable direction for future research, offering potential improvements in efficiency and versatility.

BSDF Model. We evaluated both the Ward BRDF model and the Microfacet BRDF model, and our findings indicate that both models perform effectively within our method. However, our current work is limited to isotropic materials.

In future research, we aim to extend our approach to incorporate more complex BSDF models, such as layered BRDFs, subsurface scattering materials, and

Table 1: Comparing, Liu’s method (Liu et al., 2023), and our Adaptive sampler using all test Materials. The proposed method is in blue and best values are in bold. Note samples of Liu’s method is in Rusinkiewicz parameterization($(\phi_d, \theta_h, \theta_d)$) (Rusinkiewicz, 1998), while our sample’s location is in spherical coordinates($(\theta_{in}, \phi_{in}, \theta_{out}, \phi_{out})$).

Test	Method	Liu (Liu et al., 2023)			Method	Image-based Adaptive	
Materials	Samples Count	RMSE	PSNR	Samples Number	RMSE	PSNR	
Alum-bronze	32	0.00154	36.26	$1 \times 8 \times 2 \times 2$	0.055	25.1	
	128	0.00142	36.97	$1 \times 8 \times 4 \times 4$	0.037	28.53	
	512	0.016	35.86	$1 \times 8 \times 8 \times 8$	0.02	33.84	
Dark-red-paint	32	0.0167	35.44	$1 \times 8 \times 2 \times 2$	0.026	31.8	
	128	0.0239	32.43	$1 \times 8 \times 4 \times 4$	0.0156	36.13	
	512	0.026	31.68	$1 \times 8 \times 8 \times 8$	0.016	35.68	
Color-changing-paint3	32	0.044	27.23	$1 \times 8 \times 2 \times 2$	0.049	26.18	
	128	0.0335	29.5	$1 \times 8 \times 4 \times 4$	0.06	24.43	
	512	0.0249	32.1	$1 \times 8 \times 8 \times 8$	0.033	29.54	
Dark-specular-fabric	32	0.026	31.56	$1 \times 8 \times 2 \times 2$	0.032	29.95	
	128	0.034	29.44	$1 \times 8 \times 4 \times 4$	0.012	38.43	
	512	0.033	29.7	$1 \times 8 \times 8 \times 8$	0.015	36.45	
Green-acrylic	32	0.03	30.5	$1 \times 8 \times 2 \times 2$	0.046	26.76	
	128	0.07	23.1	$1 \times 8 \times 4 \times 4$	0.044	27.21	
	512	0.05	26	$1 \times 8 \times 8 \times 8$	0.043	27.26	
Pink-fabric	32	0.02	33.94	$1 \times 8 \times 2 \times 2$	0.04	27.853	
	128	0.02	33.92	$1 \times 8 \times 4 \times 4$	0.025	32.16	
	512	0.026	31.53	$1 \times 8 \times 8 \times 8$	0.0234	32.62	
Red-fabric2	32	0.025	32.1	$1 \times 8 \times 2 \times 2$	0.024	32.49	
	128	0.032	30	$1 \times 8 \times 4 \times 4$	0.01	39.72	
	512	0.035	29.2	$1 \times 8 \times 8 \times 8$	0.0098	40.17	
Green-metallic-paint	32	0.067	23.42	$1 \times 8 \times 2 \times 2$	0.056	25	
	128	0.028	31.13	$1 \times 8 \times 4 \times 4$	0.0246	32.17	
	512	0.0271	31.32	$1 \times 8 \times 8 \times 8$	0.02	33.94	
White-diffuse-bball	32	0.04	28.47	$1 \times 8 \times 2 \times 2$	0.0221	30.36	
	128	0.038	28.3	$1 \times 8 \times 4 \times 4$	0.031	30.22	
	512	0.022	32.98	$1 \times 8 \times 8 \times 8$	0.029	30.65	
Specular-orange-phenolic	32	0.039	28.2	$1 \times 8 \times 2 \times 2$	0.077	22.3	
	128	0.062	24.1	$1 \times 8 \times 4 \times 4$	0.053	25.57	
	512	0.0462	26.71	$1 \times 8 \times 8 \times 8$	0.0345	29.2	
Red-metallic-paint	32	0.04	28	$1 \times 8 \times 2 \times 2$	0.081	21.86	
	128	0.05	26.2	$1 \times 8 \times 4 \times 4$	0.058	24.7	
	512	0.04	27.5	$1 \times 8 \times 8 \times 8$	0.0294	30.6	
Pink-plastic	32	0.013	37.92	$1 \times 8 \times 2 \times 2$	0.078	23.25	
	128	0.02	33.99	$1 \times 8 \times 4 \times 4$	0.048	26.42	
	512	0.019	34.58	$1 \times 8 \times 8 \times 8$	0.019	34.56	
PVC	32	0.038	28.44	$1 \times 8 \times 2 \times 2$	0.064	23.83	
	128	0.03	30	$1 \times 8 \times 4 \times 4$	0.046	26.71	
	512	0.031	30.2	$1 \times 8 \times 8 \times 8$	0.023	32.8	
Light-red-paint	32	0.018	34.85	$1 \times 8 \times 2 \times 2$	0.082	21.76	
	128	0.029	30.82	$1 \times 8 \times 4 \times 4$	0.042	27.52	
	512	0.0283	31	$1 \times 8 \times 8 \times 8$	0.025	31.94	
Maroon-plastic	32	0.033	29.65	$1 \times 8 \times 2 \times 2$	0.068	23.25	
	128	0.063	24.1	$1 \times 8 \times 4 \times 4$	0.054	25.3	
	512	0.04	27.4	$1 \times 8 \times 8 \times 8$	0.03	30.4	

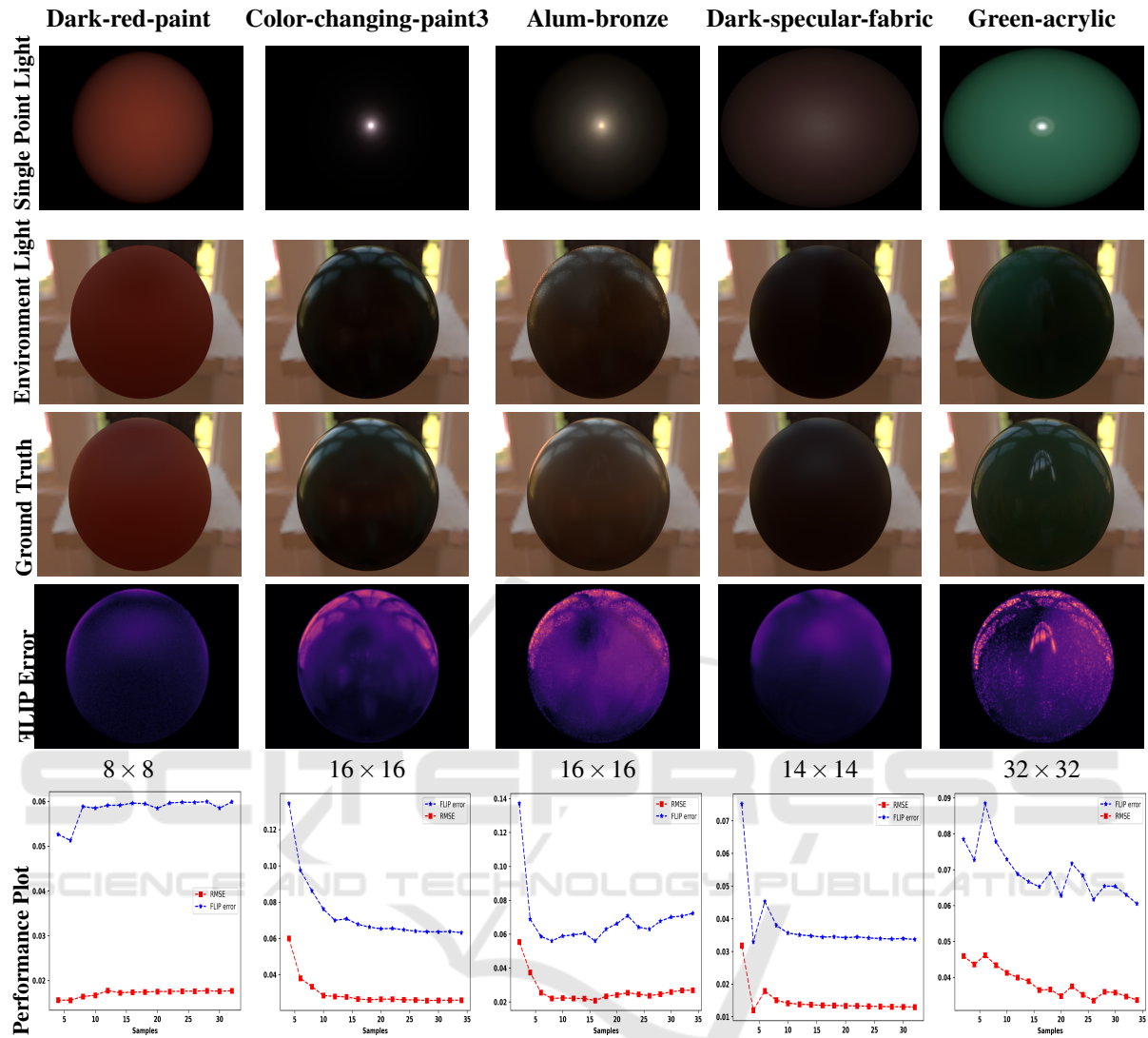


Figure 5: Rendered sphere of Five Different Materials from the MERL Dataset. The first row shows our measurements rendered under single-point lighting. The second row shows our measurements rendered under environmental lighting. The third row shows the ground truth rendered under the same environmental lighting conditions. The fourth row shows the \mathcal{FLIP} error images between the second and third rows. The final row presents a plot of error metric values versus the number of samples for each material. The Y-axis of final row represents the RMSE and \mathcal{FLIP} error values, while the X-axis indicates the sample counts, ranging from 2×2 to 32×32 of outgoing directions.

anisotropic materials. We believe the adaptive capabilities of our method could be further leveraged to handle these complicated material representations effectively.

7 CONCLUSION

We propose an image-based adaptive BRDF sampling method that significantly reduces BRDF measurement time while maintaining high accuracy and

fidelity. We use a lightweight neural network and show that it can accurately estimate BRDF parameters and that this, in turn, can be used to importance sample new directions for taking measurements. We validate our approach using both the MERL dataset and the Ward BRDF model. Additionally, we compare our method against the state-of-the-art method by Liu et al (Liu et al., 2023).

Our method demonstrates some improved performance in some aspects. By adaptively sampling each material independently, without relying on references from other materials, our technique ensures that addi-

tional measured samples directly contribute to a more accurate BRDF representation. This characteristic distinguishes our method from previous approaches and results in a more robust representation. Consequently, our approach exhibits enhanced reliability.

ACKNOWLEDGEMENTS

This project has received funding from the European Union's Horizon 2020 research and innovation program under Marie Skłodowska-Curie grant agreement No956585. We thank the anonymous reviewers for their feedback.

REFERENCES

- Andersson, P., Nilsson, J., Akenine-Möller, T., Oskarsson, M., Åström, K., and Fairchild, M. D. (2020). FLIP: A Difference Evaluator for Alternating Images. *Proceedings of the ACM on Computer Graphics and Interactive Techniques*, 3(2):15:1–15:23.
- Bai, Y., Wu, S., Zeng, Z., Wang, B., and Yan, L.-Q. (2023). BsdF importance baking: A lightweight neural solution to importance sampling general parametric bsdfs.
- Cook, R. L. and Torrance, K. E. (1982). A reflectance model for computer graphics. *ACM Transactions on Graphics (ToG)*, 1(1):7–24.
- Deschaintre, V., Aittala, M., Durand, F., Drettakis, G., and Bousseau, A. (2019). Flexible svbrdf capture with a multi-image deep network.
- Dupuy, J. (2015). *Photorealistic Surface Rendering with Microfacet Theory*. PhD thesis.
- Dupuy, J. and Jakob, W. (2018). An adaptive parameterization for efficient material acquisition and rendering. *ACM Transactions on Graphics*, 37(6):1–14.
- Foo, S. C. et al. (1997). *A gonioreflectometer for measuring the bidirectional reflectance of material for use in illumination computation*. PhD thesis, Citeseer.
- Gao, D., Li, X., Dong, Y., Peers, P., Xu, K., and Tong, X. (2019). Deep inverse rendering for high-resolution SVBRDF estimation from an arbitrary number of images. *ACM Transactions on Graphics*, 38(4):1–15.
- Jakob, W., Speierer, S., Roussel, N., Nimier-David, M., Vicini, D., Zeltner, T., Nicolet, B., Crespo, M., Leroy, V., and Zhang, Z. (2022). Mitsuba 3 renderer. <https://mitsuba-renderer.org>.
- Kavoosighafi, B., Hajisharif, S., Miandji, E., Baravdish, G., Cao, W., and Unger, J. (2024). Deep svbrdf acquisition and modelling: A survey. *Computer Graphics Forum*, 43.
- Liu, C., Fischer, M., and Ritschel, T. (2023). Learning to learn and sample brdfs. *Computer Graphics Forum (Proceedings of Eurographics)*, 42(2):201–211.
- Matusik, W., Pfister, H., Brand, M., and McMillan, L. (2003). A data-driven reflectance model. *ACM Trans. Graph.*, 22(3):759–769.
- Miandji, E., Tongbuasirilai, T., Hajisharif, S., Kavoosighafi, B., and Unger, J. (2024). Frost-brdf: A fast and robust optimal sampling technique for brdf acquisition. *IEEE transactions on visualization and computer graphics*, PP.
- Müller, T., McWilliams, B., Rousselle, F., Gross, M., and Novák, J. (2019). Neural Importance Sampling. *ACM Transactions on Graphics*, 38(5):1–19.
- Nicodemus, F. E. (1965). Directional reflectance and emissivity of an opaque surface. *Applied optics*, 4(7):767–775.
- Nielsen, J. B., Jensen, H. W., and Ramamoorthi, R. (2015). On optimal, minimal BRDF sampling for reflectance acquisition. *ACM Transactions on Graphics*, 34(6):1–11.
- Phong, B. T. (1975). Illumination for computer generated pictures. *Commun. ACM*, 18(6):311–317.
- Rusinkiewicz, S. M. (1998). A new change of variables for efficient brdf representation. In *Rendering Techniques '98: Proceedings of the Eurographics Workshop in Vienna, Austria, June 29–July 1, 1998*, 9, pages 11–22. Springer.
- Walter, B. (2005). Notes on the ward brdf. <https://www.graphics.cornell.edu/bjw/wardnotes.pdf>.
- Zeng, Z., Deschaintre, V., Georgiev, I., Hold-Geoffroy, Y., Hu, Y., Luan, F., Yan, L.-Q., and Hašan, M. (2024). Rgb \leftrightarrow x: Image decomposition and synthesis using material- and lighting-aware diffusion models. In *ACM SIGGRAPH 2024 Conference Papers, SIGGRAPH '24*, New York, NY, USA. Association for Computing Machinery.
- Zhang, X., Srinivasan, P. P., Deng, B., Debevec, P., Freeman, W. T., and Barron, J. T. (2021). NeRFactor: neural factorization of shape and reflectance under an unknown illumination. *ACM Transactions on Graphics*, 40(6):1–18.